

# Optical properties of rodlike and bipyramidal gold nanoparticles from three-dimensional computations

Mingzhao Liu and Philippe Guyot-Sionnest\*

*James Franck Institute, The University of Chicago, Chicago, Illinois 60637, USA*Tae-Woo Lee<sup>†</sup> and Stephen K. Gray<sup>‡</sup>*Chemistry Division and Center for Nanoscale Materials, Argonne National Laboratory, Argonne, Illinois 60439, USA*

(Received 28 August 2007; revised manuscript received 2 November 2007; published 26 December 2007)

Near- and far-field optical properties of several types of gold nanoparticle are investigated with rigorous three-dimensional computational electrodynamics. The primary focus is on the results obtained with the finite-difference time-domain method, although some results obtained with the discrete dipole approximation are also given. We first consider spheres and prolate spheroids, where analytical solutions are available for comparison. The spectra of gold nanorods and pentagonal bipyramids are then investigated and excellent agreement with recent experimental optical spectra is found. The local field enhancement ( $|\mathbf{E}|/|\mathbf{E}_0|$ ) is studied at the longitudinal plasmon resonance. Sharper structural features produce more significant enhancement and the largest enhancement of more than a factor of 200 is seen around the poles of the bipyramid. The fields within the nanoparticles are also studied. Whereas the field magnitude is nearly uniform within small spheres and spheroids, it can be nonuniform for nanorods and bipyramids. The field magnitude decreases from the center toward the poles in the case of nanorods, but increases rapidly in the case of bipyramids. A large internal field enhancement by more than a factor of 30 is seen for the bipyramids, which suggests that these particles will exhibit strong optical nonlinearities.

DOI: 10.1103/PhysRevB.76.235428

PACS number(s): 78.67.Bf

## I. INTRODUCTION

It has been known for some time that noble metals, i.e., elements in group IB, display distinct colors when dispersed as nanoparticles in transparent media.<sup>1</sup> This phenomenon arises from the optical excitation of surface plasmons, which leads to strong light absorption and scattering at resonant frequencies.<sup>2,3</sup> At the plasmon resonance, the near field of the nanoparticles is disturbed, giving rise to a large local field enhancement which allows electromagnetic energy to be focused more tightly than the diffraction limit which applies to conventional optics. This enhanced electromagnetic field couples strongly with electronic transitions, leading to surface-enhanced Raman scattering<sup>4</sup> (SERS) as well as the optical antenna effect.<sup>5</sup> Optical nonlinearity can also arise from the local field enhancement, allowing the active control of light propagation in a plasmonic waveguides.<sup>6</sup> The plasmon modes of a metal particle are determined by its shape, composition, size, and surrounding medium. In recent years, metal nanoparticles with different shapes have been synthesized and studied optically. The shapes explored include prisms,<sup>7</sup> shells,<sup>8</sup> cubes,<sup>9</sup> bipyramids,<sup>10</sup> and rods,<sup>11,12</sup> tuning their plasmon modes across the whole visible and near-infrared range. Elongated nanoparticles such as nanorods or bipyramids are especially promising systems for optical studies as their spectra are easily tunable by varying the aspect ratio. Compared to spheres with the same volume, rodlike structures also give a larger curvature at the tips, where significant field enhancement is expected.

Although the optical process involved is excitation of a plasmon, which is a collective oscillation of electrons near the metal surface,<sup>13</sup> it is often well approximated with classical electrodynamics. The quantum mechanical aspects of

the process are integrated into a phenomenological permittivity  $\epsilon(\lambda)$  of the metal. This was first shown by Mie, who solved the problem of plane electromagnetic wave scattering by a homogeneous dielectric sphere exactly and completely.<sup>14</sup> The solution explains the spectrum of spherical gold colloids accurately, although correction for surface effect is necessary for very small particles ( $d < 5$  nm).<sup>15</sup> More generally, an analytical solution has been developed for the spheroid, which includes the sphere and infinite-long cylinder as special cases.<sup>3</sup>

For many nanoparticle shapes, however, analytical solutions are not available. The lack of an analytical solution sets a barrier to understanding their spectra quantitatively and to gaining further insight into their near-field properties. Different methods have been developed to solve Maxwell's equations numerically, including the *T*-matrix method,<sup>16,17</sup> the discrete dipole approximation (DDA),<sup>18,19</sup> and the finite-difference time-domain method (FDTD).<sup>20,21</sup> The *T*-matrix method emphasizes more the far-field properties, i.e., the scattered field, and it is better developed for systems with revolution symmetry. The DDA and FDTD methods, however, can give both near- and far-field properties due to their finite-element nature. Indeed, there have been extensive DDA calculations reported by Schatz and co-workers, showing it to be a powerful tool to calculate the spectra as well as the near-field properties of metal colloids.<sup>22–24</sup>

Our main purpose is to discuss the optical properties of rodlike and bipyramidal gold nanoparticles using the FDTD method. FDTD methodology is well developed and has been applied to many systems.<sup>25,26</sup> The FDTD method calculates the time evolution of electromagnetic fields, making it complementary to frequency-domain methods such as DDA. We also present DDA results which allows us to infer some

relative pros and cons of the methods. Our calculations lead to optical spectra that agree well with recent experimental results and we also examine the near field enhancements of the electromagnetic fields.

The electromagnetic fields *inside* metal nanoparticles have attracted little attention. This is because they cannot be directly probed experimentally and the coupling between plasmons and other electronic systems as in, e.g., SERS, is accomplished with exterior near fields. However, internal field distributions are relevant to the nonlinear optical response of the particles and deserve further study. In this paper, we determine accurate interior fields and find that the bipyramidal metal nanoparticles should be particularly promising candidates for exhibiting nonlinear optical properties.

## II. COMPUTATIONAL METHODS

The FDTD method solves the time-dependent Maxwell's equations by discretizing space and time and involves a relatively simple time-stepping algorithm. For the optical properties of nonmagnetic metal nanoparticles with a given geometry, the only parameters required for the calculation are the dielectric constants of the metal particle and the medium, which are usually obtained as phenomenological values by other optical measurements. The dielectric constants of metals are complex valued and strongly dispersive, i.e.,  $\epsilon(\omega) = \epsilon_r(\omega) + i\epsilon_i(\omega)$ , which requires special care to be properly implemented within the FDTD method.<sup>25</sup> However, it is easy to see that one of Maxwell's equations,

$$\nabla \times \mathbf{H}(\omega) = -i\omega \mathbf{D}(\omega) = -i\omega \epsilon_0 \epsilon(\omega) \mathbf{E}(\omega),$$

can be written in an equivalent form of

$$\nabla \times \mathbf{H}(\omega) = -i\omega \left[ \epsilon_0 \epsilon_\infty \mathbf{E}(\omega) + \sum_{i=0}^N \mathbf{P}_i(\omega) \right],$$

if one expresses the relative dielectric constant of the metal as  $\epsilon(\omega) = \epsilon_\infty + \sum_{i=0}^N \chi_i(\omega)$ , and defines polarizations  $\mathbf{P}_i(\omega) = \epsilon_0 \chi_i(\omega) \mathbf{E}(\omega)$ . Once an analytical form for each  $\chi_i(\omega)$  is specified, the differential equations to determine  $\mathbf{P}_i(t)$  can be found by Fourier transformation of  $\mathbf{P}_i(\omega)$  into the time domain. Thereafter, the following time-dependent form of Maxwell's equations,

$$\nabla \times \mathbf{H}(t) = \frac{\partial}{\partial t} \mathbf{D}(t) = \epsilon_0 \epsilon_\infty \frac{\partial}{\partial t} \mathbf{E}(t) + \frac{\partial}{\partial t} \sum_{i=0}^N \mathbf{P}_i(t), \quad (1)$$

$$\frac{\partial}{\partial t} \mathbf{H}(t) = -\frac{1}{\mu_0} \nabla \times \mathbf{E}(t), \quad (2)$$

can be solved stably by the FDTD method using the auxiliary differential equation approach.<sup>21</sup>

In order to account for both the free electron plasmon and interband transitions, we take the dielectric function,  $\epsilon(\omega)$ , for gold to be the sum of a Drude term and several Lorentzian terms.<sup>3</sup> In particular, we fit  $\epsilon(\omega)$  to a combination of experimental data available from Palik's handbook (the Lynch-Hunter data set)<sup>27</sup> and Johnson and Christy<sup>28</sup> within

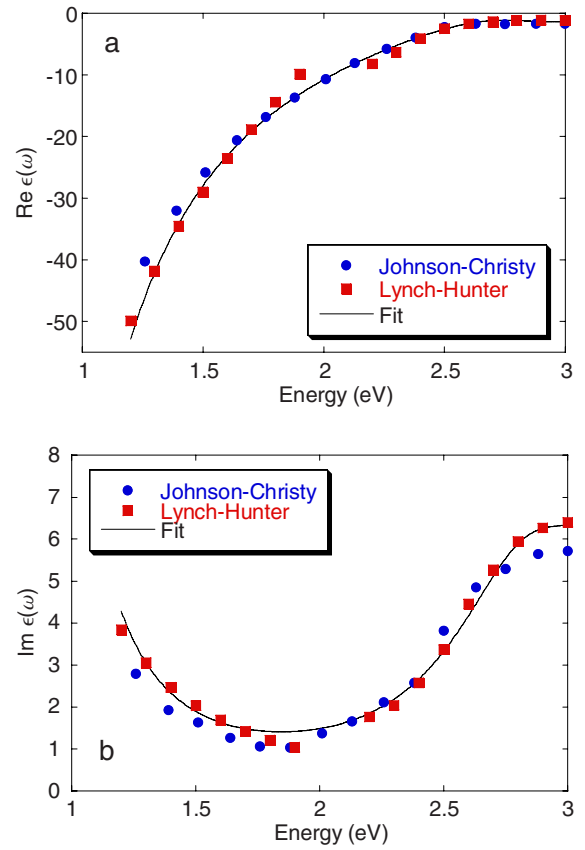


FIG. 1. (Color online) Symbols denote empirical dielectric constant data for gold  $\epsilon(\omega) = \text{Re } \epsilon(\omega) + i \text{Im } \epsilon(\omega)$  and the solid curves represent the fit given by Eq. (3). In our fit we used primarily Lynch and Hunter's assessment in the Palik handbook<sup>27</sup> except for the 1.9–2.3 eV range where we used the Johnson-Christy (Ref. 28) data (see text for more detail).

the 1.2–3 eV range (Fig. 1) using the following model:

$$\epsilon(\omega) = \epsilon_\infty - \frac{\omega_D^2}{\omega^2 + i\omega\gamma_D} - \sum_{k=1}^3 \frac{g_{L,k} \omega_{L,k}^2 \Delta\epsilon}{\omega^2 - \omega_{L,k}^2 + 2i\omega\gamma_{L,k}}. \quad (3)$$

With the exception of the 1.9–2.3 eV range, we fit Eq. (3) to Lynch and Hunter's recommended values.<sup>27</sup> It is important to note that this data has anomalous behavior in the 1.9–2.3 eV range ( $\lambda = 652\text{--}539$  nm). This anomaly has also been recently noted elsewhere.<sup>29</sup> We therefore used the data from Johnson and Christy<sup>28</sup> in the 1.9–2.3 eV range, which does not show this anomaly.

In accordance to the model above, the polarization vectors  $\mathbf{P}_i(t)$  are determined by the following equations:

$$\left( \frac{\partial^2}{\partial t^2} + \gamma_D \frac{\partial}{\partial t} \right) \mathbf{P}_0(t) = \epsilon_0 \omega_D^2 \mathbf{E}(t), \quad (4)$$

$$\left( \frac{\partial^2}{\partial t^2} + 2\gamma_{L,k} \frac{\partial}{\partial t} + \omega_{L,k}^2 \right) \mathbf{P}_k(t) = g_{L,k} \omega_{L,k}^2 \Delta\epsilon \mathbf{E}(t), \quad (5)$$

where  $k = 1, 2$ , or  $3$ . With Eqs. (1), (2), (4), and (5), the field vectors and polarization vectors can be calculated in a stan-

standard FDTD propagation scheme with other details (total field and/or scattered field injection of the initial wave packet and absorbing boundary conditions) as discussed elsewhere.<sup>21</sup> The above equations apply to the region of space occupied by the metal nanoparticle. The medium is characterized simply as a dielectric with a positive and nondispersive dielectric constant  $\epsilon_m$  [Eqs. (1) and (2), with no polarization vectors and  $\epsilon_\infty$  replaced by  $\epsilon_m$  apply]. If not specified, it is set to be that of water with  $\epsilon_m = 1.77$  (i.e., refractive index of 1.33) in the calculations discussed below.

The FDTD calculations are performed on the Jazz cluster at Argonne National Laboratory, which has 350 nodes each equipped with an Intel Xeon 2.4 GHz processor and at least 1 Gbyte random access memory (RAM). Depending on the problem size, a parallel calculation is carried on 2–45 nodes, which allows a simulation to be done within 24 h.

The DDA calculations<sup>18,19</sup> were performed with an appropriate adaptation of the program written by Draine and Flatau.<sup>30</sup> These calculations involved simple cubic lattices, grid spacings similar to the FDTD calculations, and a small ( $\epsilon = 10^{-6}$ ) error tolerance for convergence of the iterations. The calculations are carried out on a 16-node cluster where each node has two AMD Athlon 1900+ processors and 2 Gbytes RAM.

### III. OPTICAL SPECTRA OF GOLD NANOPARTICLES WITH DIFFERENT SHAPES

#### A. Spherical nanoparticles

The scattering of a plane electromagnetic wave by a spherical object has been solved analytically by Mie and Lorenz, in equivalent forms.<sup>14</sup> For the Mie solution, we used the code given by Bohren and Huffman to calculate the absorption spectra of gold nanospheres with different sizes.<sup>3</sup> The results are shown in Fig. 2(a). The spectra calculated for the same systems with FDTD are shown in Fig. 2(b). One can see that the FDTD simulation reproduces the analytical results very well, both on the line shapes and the cross section at the plasmon resonances. The FDTD plasmon resonance of the 10 nm radius gold nanoparticle (2.38 eV) agrees with the expectation (2.39 eV) of the quasistatic approximation [ $\text{Re } \epsilon(\omega) = -2\epsilon_m$ ] very well, as a result of its smaller size. However, the plasmon resonance redshifts and broadens as the gold nanoparticle grows larger due to the phase retardation and the increasing contribution from higher order modes. The peaks are located at 2.35 eV for the 25 nm radius particle and 2.29 eV for the 50 nm radius particle. In the quasistatic approximation, the optical absorption cross section is proportional to the volume of the particle; therefore, the absorption efficiency  $Q_{\text{abs}} = C_{\text{abs}} / \pi r^2$  is proportional to its radius. This relation holds roughly for the gold nanoparticles with radii 10 nm and 25 nm. However, the retardation effect becomes so significant for the 50 nm radius gold nanoparticle that its absorption efficiency at resonance is even lower than the 25 nm radius gold nanoparticle. The DDA method has also been shown to give quite good results for similar problems,<sup>22</sup> although we found that the cross sections are consistently less ( $\sim 10\%$ ) than the Mie theory expectations.

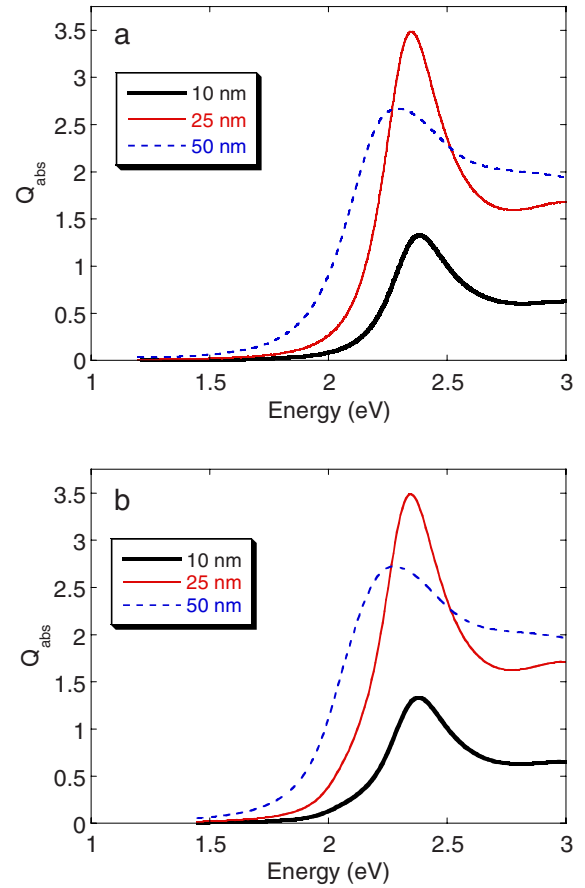


FIG. 2. (Color online) Absorption spectra of spherical gold nanoparticles with radii of 10, 25, and 50 nm, all immersed in water ( $n=1.33$ ): (a) Mie's solution and (b) FDTD results.  $Q_{\text{abs}}$  is the absorption cross section normalized by the geometrical cross section  $\pi r^2$ . In the FDTD calculations, the spatial resolution was set as either 0.5 nm (for 10 nm sphere) or 1 nm (for the 25 and 50 nm spheres).

#### B. Spheroidal nanoparticles

Optical scattering by an ellipsoid is the next simplest that can be solved analytically since the boundary conditions can be treated in ellipsoidal coordinates. It was shown by Gans that a homogeneous and isotropic ellipsoid is homogeneously polarized in the quasistatic limit.<sup>31</sup> The polarizabilities along the three principal axes are

$$\alpha_i = V \frac{\epsilon - \epsilon_m}{\epsilon_m + L_i(\epsilon - \epsilon_m)} \quad (i = 1, 2, 3),$$

where  $V$  is the volume of the ellipsoid,  $\epsilon$  and  $\epsilon_m$  are, respectively, the dielectric constants of the ellipsoid and the medium, and  $L_i$  are geometric factors defined as

$$L_i = \frac{1}{2} \int_0^\infty dq \prod_{j=1}^3 a_j (a_j^2 + q)^{-(\delta_{ij} + 1/2)},$$

where  $a_1 \leq a_2 \leq a_3$  are the semiaxes of the ellipsoid and  $\delta_{ij}$  is the Kronecker delta.<sup>3</sup> For a sphere, for example,  $L_1 = L_2 = L_3$

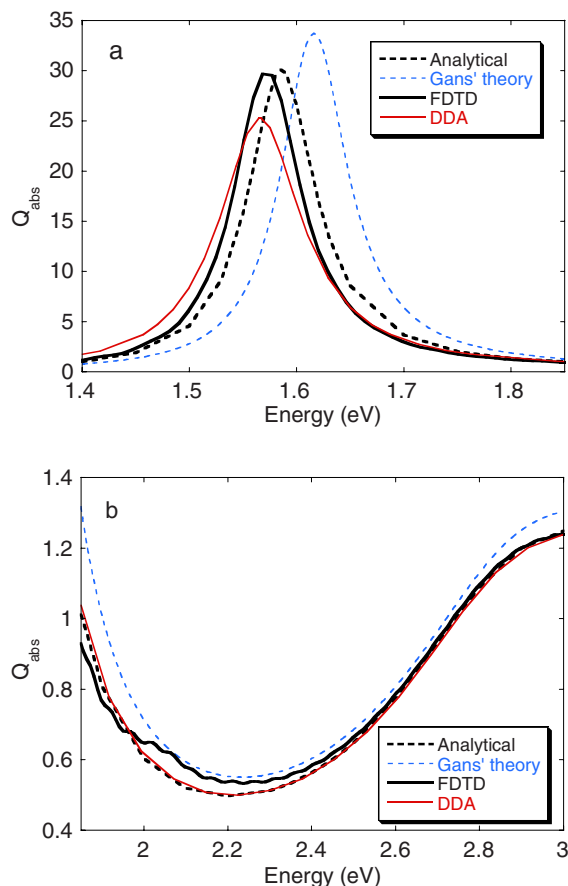


FIG. 3. (Color online) Absorption spectrum of a gold prolate spheroid with minor axis of 14 nm and aspect ratio of 4.1 calculated by different methods: the analytical solution of Voshchinnikov and Farafonov (bold black dashed line), Gans' quasistatic approximation (blue dashed line), FDTD simulation (bold black line), and DDA simulation (red line). The incident light polarization is along the major axis of the spheroid. Panel (a) shows the spectrum in the 1.4–1.85 eV range and panel (b) shows the 1.85–3 eV range. In panel (b) the DDA result and analytical result coincide with each other. The small oscillation shown on the FDTD result in panel (b) is because a finite time window is used to collect the scattered wave, which produces a small ringing artifact in its Fourier transformation into the frequency domain.

$= 1/3$ . The absorption cross sections with polarization along axis  $i$  are then given by the optical theorem,

$$C_{abs} = k \text{Im } \alpha_i,$$

where  $k$  is the wave number of the incident light. This model is still used nowadays to explain the spectra from elongated nanoparticles, most commonly, nanorods. The solution for spheroid ( $a_1 = a_2$ ) in the general case, i.e., finite wavelength to size ratio, was given by Asano and Yamamoto.<sup>32</sup> Later, a new solution was given by Voshchinnikov and Farafonov which is more computationally efficient.<sup>33</sup> This solution was developed for scattering problems and therefore only the far-field behavior was addressed.

In Fig. 3, we plot the absorption spectrum of a prolate

spheroid ( $a_1 = a_2 < a_3$ ) with minor axis of 14 nm and aspect ratio of 4.1 using Gans' solution, the exact analytical solution of Voshchinnikov and Farafonov, the DDA and FDTD methods. The fitted dielectric function shown in Fig. 1 is used for all the calculations. The incident light polarization is along the major axis of the ellipsoid, so the spectrum of the longitudinal mode is being probed. The exact analytical solution shows that the longitudinal plasmon mode is at 1.588 eV, with absorption efficiency  $Q_{abs} \approx 30$ . The efficiency is a dimensionless quantity defined as the optical cross section  $C_{abs}$  divided by the effective geometrical cross section  $\pi a^2$ , where the effective radius  $a \equiv (3V/4\pi)^{1/3}$ . In Gans' quasistatic solution, the resonance is noticeably blueshifted to 1.616 eV, with the absorption efficiency  $Q_{abs}$  being about 10% larger than the exact result. Such differences contrast with typical expectations that the higher order modes are negligible since the dimension of the spheroid in the wave propagation direction (14 nm) is much smaller than the resonance wavelength ( $\sim 780$  nm). The quasistatic limit linewidth, however, is in accord with the exact result, 77 meV.

The FDTD spectrum obtained with 1 nm grid resolution shows a resonance at 1.560 eV, with absorption efficiency similar to the exact result. The resonance is redshifted by 28 meV relative to the exact solution. The shift is reduced by half to 14 meV using a 0.5 nm grid resolution, indicating that the FDTD simulation is converging to the analytical solution. Both calculations give a linewidth of 76 meV, matching the analytical result very well. For comparison purposes, the absorption spectrum was also calculated with DDA.<sup>18,19,30</sup> The result shows the plasmon resonance at 1.567 eV, similar to the FDTD result. The DDA result converges very nicely to the analytical result at higher energies ( $> 1.7$  eV). However, the absorption efficiency is about 17% smaller than the analytical result. It has been noted that better convergence can be achieved by further reducing the grid size to 0.25 nm.<sup>24</sup> However, we find that the accuracy in this case is only slightly improved relative to that in Fig. 3. The underestimate of the cross section near resonance by the DDA method is most likely due to the fact that it is known that the DDA method is less appropriate (i.e., will converge more slowly) in the limit of large index of refractions magnitudes,  $|n| \equiv |\sqrt{\epsilon}|$ .<sup>19</sup> Near the plasmon resonance in Fig. 3(a) ( $E \approx 1.5$  eV),  $|n|$  is about 5.4, and increases rapidly toward lower energy (Fig. 1). This is also consistent with the fact that the DDA cross sections are much more accurate at higher energies where  $|n|$  is significantly smaller [Fig. 3(b)].

A few remarks on the relative pros and cons of DDA and FDTD simulations are in order. We have found that FDTD calculations can be more time consuming than DDA ones with the same grid resolution. For example, it takes about 600 node hours (i.e., computation time multiplied by the number of nodes employed) for the FDTD to obtain the spectrum shown in Fig. 3. For a frequency-domain DDA simulation, the computation time depends on the frequency significantly. At 0.5 nm resolution DDA requires only a few minutes for each frequency at 2–3 eV, but around 1 h in the 1–2 eV range due to the convergence difficulties in this region. Altogether, it takes about 100 node hours for the DDA calculation to get the full spectrum of interest at a 10 meV



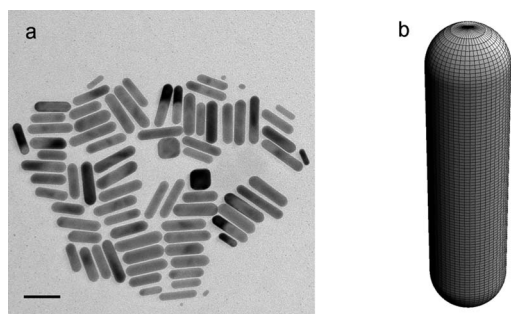


FIG. 4. (a) TEM image of gold nanorods synthesized by a seed-mediated method and (b) the idealized 3D model assumed for our calculations. Scale bar=50 nm.

energy resolution. Therefore, DDA is clearly a better method in the high energy range (2–3 eV) due to its accuracy and fast convergence. While still faster than the FDTD method at lower energies, there can be some loss of accuracy in the DDA results, as noted in the paragraph above. The large amounts of computer time involved in all these calculations is required to achieve very high accuracy and quantitative agreement with experimental results for the nanorod and bipyramid particles to be discussed later. If one is satisfied with 10%–20% agreement in peak positions and intensities, considerably larger grid spacings could be employed. A grid resolution of 2 nm, for example, four times larger than the 0.5 nm we prefer for high accuracy, results in FDTD simulations that are about 128 times faster when both the fewer number of spatial and time grid points are considered.

### C. Rod-shape nanoparticles

Although spheroidal metal nanoparticles are good from the perspective of analytical calculations, there are very few experimental studies available on them due to the difficulty in chemical synthesis and separation of such particles. Gold nanorods, however, have been synthesized by various methods as a replacement to prolate spheroids.<sup>10–12</sup> Their optical properties have been studied extensively at both the ensemble and single-particle level, and small nanorods can be approximated by Gans' theory of small ellipsoidal particles. Recently, their ultrafast nonlinear optical properties have been studied with pump-probe techniques, and up to 20% pump-induced change in scattering cross section was observed.<sup>6</sup>

For the FDTD simulations, the nanorod is modeled as a finite cylinder with both ends capped by hemispheres (Fig. 4). The nanorod modeled this way is very close in shape to the nanorods observed in transmission electron microscopy (TEM). The aspect ratio of a nanorod is defined as the ratio between its total length and diameter. The diameter of the nanorods is fixed at 14 nm, as typically observed from experiment.<sup>10–12</sup> The grid resolution is chosen to be 0.5 nm, matching the accuracy level of that of the spheroid calculations above. The simulations are performed for three aspect ratios of 3.4, 4.1, and 4.8 and give resonance energies (wavelengths) as 1.67 eV (741 nm), 1.53 eV (808 nm), and 1.41 eV (878 nm), as shown in Fig. 5(a). The longitudinal

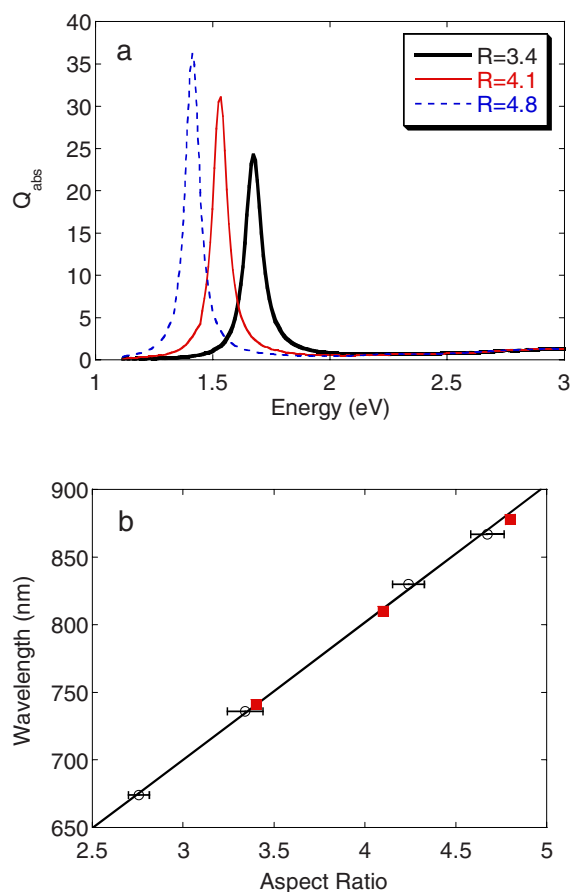


FIG. 5. (Color online) (a) Absorption spectra of gold nanorods with diameter of 14 nm and aspect ratios of 3.4, 4.1, and 4.8, calculated by FDTD simulations with 0.5 nm grid resolution and incident light polarization along the major axis of the nanorods. (b) Theoretical wavelengths of the longitudinal plasmon resonances (filled red squares) are compared with experimental values (open circles with error bars). The line is a least-squares fit to the experimental data.

plasmon resonance redshifts as the aspect ratio increases, which is consistent with the experimental results. It is found by experiment that the wavelength of the resonance varies linearly with the aspect ratio [Fig. 5(b)]. The simulation results agree with the experimental relation remarkably well. The plasmon resonance narrows as it redshifts as a result of reduced contributions from interband transitions. For the resonances at 1.67, 1.53, and 1.41 eV, the linewidths are, respectively, 84, 76, and 72 meV, respectively.

### D. Bipyramidal nanoparticles

Recently, gold nanoparticles with bipyramidal shape were synthesized in aqueous solution using a seed-mediated approach [Fig. 6(a)].<sup>10</sup> The colloidal solution has a pronounced optical absorption feature around 1.5 eV, corresponding to the longitudinal plasmon resonance of the bipyramids. The absorption feature is very narrow, with a linewidth of  $\sim 0.12$  eV, due to the monodispersity of the bipyramidal nanoparticles in their shape and size. The bipyramids have

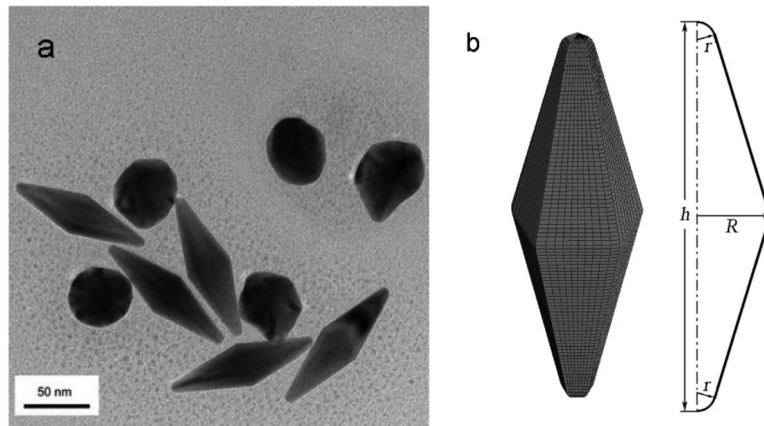


FIG. 6. (a) TEM image of gold bipyramids (some spherical-like particles are also evident). (b) 3D model of a pentagonal bipyramid (left side) and a radial cross section from its axis to one of its edges (right side).

reasonably sharp tip at their poles, which is promising for strong field enhancement. The detailed structure of the bipyramid was studied by high resolution transmission electron microscopy and found to be a pentagonal bipyramid. A three-dimensional (3D) model of the structure is shown in Fig. 6(b), with its poles being rounded to fit the shapes seen by TEM. The parameters used for the model were directly measured from the TEM images. For the spectra present in Fig. 7(a), the gold bipyramid has  $R$  (radius at the equator)=15 nm,  $h$  (total length)=83.4 nm, and  $r$  (radius at the poles)=3.0 nm. The FDTD calculations were performed with 0.5 nm grid resolution and gave a longitudinal plasmon resonance at 1.53 eV, which is in excellent agreement to the experimental extinction spectrum. The experimental extinction spectrum actually includes both optical absorption and scattering. In the case of the gold bipyramids, the FDTD simulated scattering spectrum (not shown) has the same line shape and peak position as the absorption spectrum, but contributes less than 20% to the total optical extinction. Due to the larger particle size, the calculation can also be performed at 1 nm grid size, with very small changes in the results. The linewidth of the resonance is 86 meV, broader than the corresponding spheroid with similar resonance frequency. This broadening has been also observed experimentally by dark-field microscopy and can be explained by the extra radiative damping due to the larger size of the particle.<sup>10</sup> The experimental ensemble spectrum has another significant peak around 2.3 eV. However, this peak is most likely due to the spherelike by-products in the solution, as seen in Fig. 6(a) and not due to a transverse plasmon resonance as might naively be expected. From the calculations, the actual transverse plasmon mode of the bipyramid is quite weak [Fig. 7(a)]. Experimentally, it is also known that the longitudinal plasmon mode redshifts as the tips of the bipyramid grow sharper.<sup>10</sup> Figure 7(b) shows results for varying pole radius  $r$ , keeping all the other parameters the same. It clearly shows a redshift as the tip radius varies from 4.4 to 3.0 and to 2.0 nm.

#### IV. FIELD ENHANCEMENT AT THE PLASMON RESONANCE

In FDTD simulations, the field distribution at a given frequency can be obtained by Fourier transformation of the

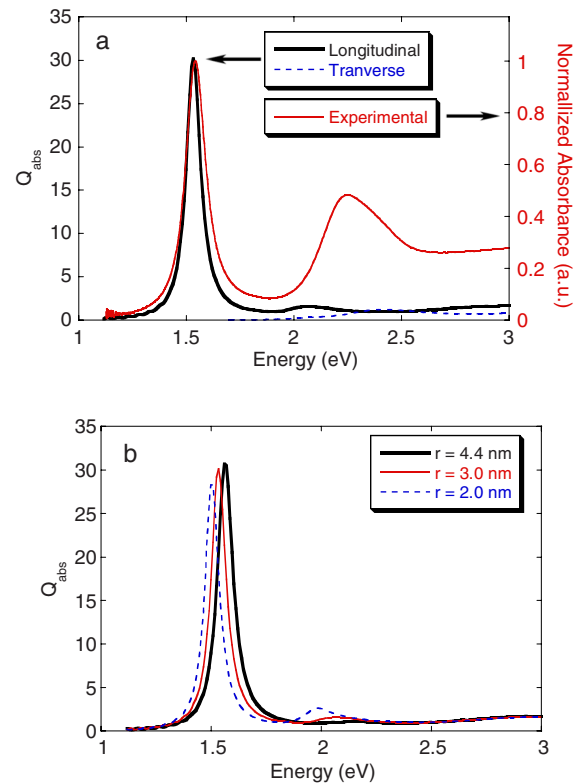


FIG. 7. (Color online) (a) The absorption spectra of a gold bipyramid with  $R=15$  nm,  $h=83.4$  nm, and  $r=3.0$  nm by FDTD simulation: longitudinal mode at 0.5 nm grid size (bold black line) and transverse mode at 1 nm grid size (blue dashed line). The experimental extinction spectrum is shown in solid red line for comparison. (b) The longitudinal plasmon resonance is redshifted as the tips of the bipyramid get sharper. There is no change on the other geometrical factors.

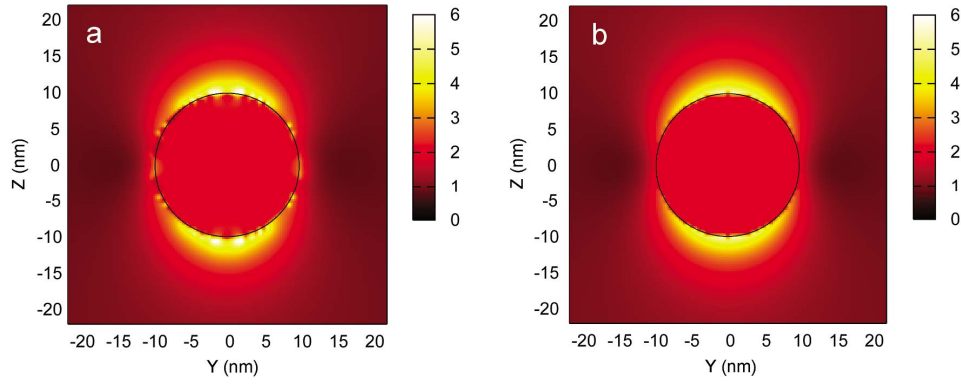


FIG. 8. (Color online) The field enhancement  $|\mathbf{E}|/|\mathbf{E}_0|$  at the plasmon resonance (2.38 eV) for a 10 nm radius gold sphere based on (a) FDTD calculation at 0.5 nm grid size and (b) quasistatic approximation. The propagation of the field is along the  $x$  axis and the polarization is along the  $z$  axis. The black ring shows the boundary of the sphere.

time-evolving field. For greater accuracy, we ran separate calculations that involved a more monochromatic incident field. The field amplitude is then normalized by the amplitude of the incident field to get the field enhancement  $|\mathbf{E}|/|\mathbf{E}_0|$ .

#### A. Spherical nanoparticles

This calculation is performed on a 10 nm radius gold sphere at its resonance frequency (2.38 eV), with the field enhancement  $|\mathbf{E}|/|\mathbf{E}_0|$  plotted in Fig. 8(a). This result can be compared with calculations based on the quasistatic approximation, which should be good enough since the size of the sphere is much smaller than the wavelength. In this approximation, the electric field around a homogeneous and isotropic sphere with radius  $a$  can be written as

$$\mathbf{E}(\mathbf{r}) = \begin{cases} \frac{3\epsilon_m}{\epsilon + 2\epsilon_m} \mathbf{E}_0 & (r \leq a) \\ \mathbf{E}_0 - \frac{\epsilon - 2\epsilon_m}{\epsilon + 2\epsilon_m} a^3 \nabla \left( \frac{\mathbf{E}_0 \cdot \mathbf{r}}{r^3} \right) & (r > a), \end{cases} \quad (6)$$

where  $\epsilon$  and  $\epsilon_m$  are, respectively, the dielectric constants of the sphere and the medium and  $\mathbf{E}_0$  is the incident electric

field. The field enhancement is then calculated for the same geometry as the FDTD simulation and shown in Fig. 8(b). The plot from the FDTD simulation is very similar to the analytical result, only producing small errors at the boundary due to the “staircasing effect,” i.e., the roughness introduced by discretizing the sphere on a cubic lattice. Both calculations show the maximum field enhancement near the surface to be about 5. The *homogeneous* internal field enhancement observed in Eq. (6) is also nicely reproduced by the FDTD simulation, with a magnitude of about 2.

#### B. Spheroidal and rod-shaped nanoparticles

Figure 9(a) shows the electric field distribution for a spheroid obtained with the FDTD method at the longitudinal plasmon resonance of 1.574 eV using a grid resolution of 0.5 nm. The near field is about the same as the analytical result recently reported by Calander and Willander.<sup>34</sup> The internal electric field enhancement is approximately uniform across the particle, with a value around 13.4. This homogeneity is followed strictly in the quasistatic approximation, in which the internal electric field of an ellipsoid is given by<sup>3</sup>

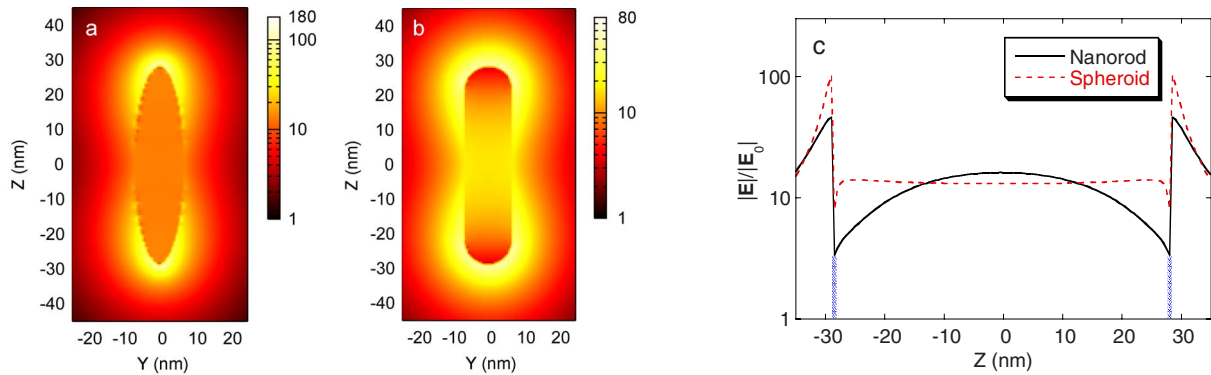


FIG. 9. (Color online) The field enhancement  $|\mathbf{E}|/|\mathbf{E}_0|$  at the plasmon resonance of a gold prolate spheroid with minor axis of 14 nm and aspect ratio of 4.1 calculated by FDTD. The propagation of the field is along the  $x$  axis and the polarization is along the  $z$  axis. (b) A similar calculation was performed on the resonance of a gold nanorod with diameter of 14 nm and aspect ratio of 4.1. (c) The field enhancement along the center axis of the nanorod (black line) is compared with an on-resonance gold prolate spheroid with diameter of 14 nm and aspect ratio of 4.1 (red dashed line). The boundary between the nanoparticle and the medium is marked by the vertical blue dotted lines.

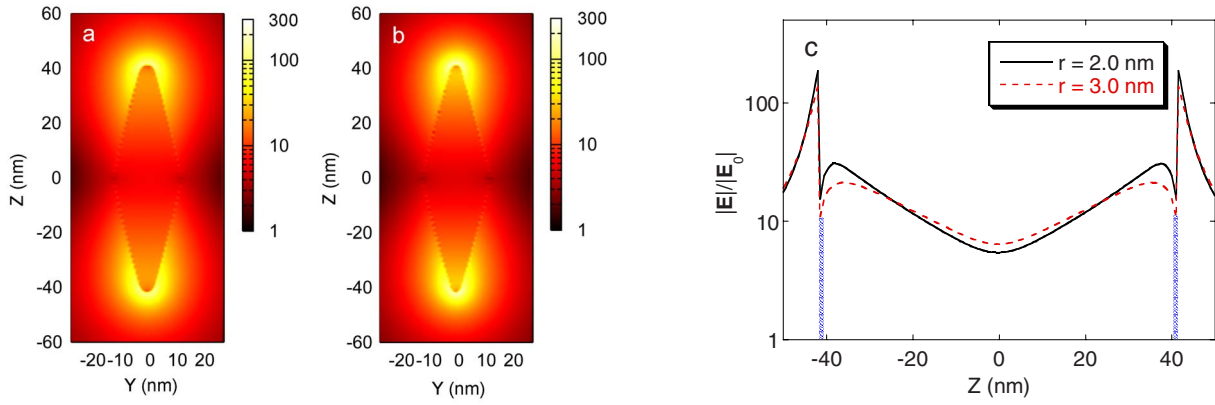


FIG. 10. (Color online) The field enhancement  $|E|/|E_0|$  at the plasmon resonances of gold bipyramids with  $R=15$  nm,  $h=83.4$  nm, and (a)  $r=3.0$  nm or (b)  $2.0$  nm. The propagation of the field is along the  $x$  axis and the polarization is along the  $z$  axis. The grid size for the FDTD calculations is  $0.5$  nm. The field enhancement along the center axes of the bipyramids are compared in panel (c). The boundary between the nanoparticle and the medium is marked by the vertical blue dotted lines.

$$\mathbf{E} = \mathbf{E}_0 + \frac{\alpha L}{V} \mathbf{E}_0 = \frac{\epsilon_m \mathbf{E}_0}{\epsilon_m + L(\epsilon - \epsilon_m)}.$$

The polarization of the prolate spheroid induces a huge local field enhancement within its vicinity. The field enhancement maxima are observed near the poles of the spheroid, to be larger than a factor of 100. In terms of field intensity  $|E|^2$ , the enhancement is thus larger than  $10^4$ . The field enhancement can be observed in quite a large region surrounding the particle. For example, there is about  $1.8 \times 10^3$  nm<sup>3</sup> of space surrounding the particle with the field intensity enhancement exceeding 1000 and about  $2.5 \times 10^4$  nm<sup>3</sup> of space with the enhancement exceeding 100, while the volume of the particle is  $8.1 \times 10^3$  nm<sup>3</sup>. We found that the corresponding DDA external field distribution (not shown) is very similar to the FDTD result. However, the field distributions within the particle were not reliable.

We also performed FDTD calculations on the cylindrical gold rod defined by Fig. 4(b), with diameter of 14 nm and aspect ratio of 4.1. The electric field distribution is calculated at its longitudinal plasmon resonance of 1.533 eV, with the grid resolution of 0.5 nm [Fig. 9(b)]. The maximum field enhancement achieved around the nanorod is significantly smaller than that of the prolate spheroid with the same aspect ratio, as a result of the smaller curvature of the nanorod at the poles. However, the comparison may favor the nanorod better if we look at the volume of field enhancement, instead of its maximum value. The region of space with field intensity enhancement exceeding 1000 has a volume of about  $2.4 \times 10^3$  nm<sup>3</sup>. However, for field intensity enhancement exceeding 100, the corresponding volume is  $4.0 \times 10^4$  nm<sup>3</sup>. Both values are comparable to the numbers given above for the case of spheroid, upon the normalization by the volumes of the particles.

The electric field intensity distribution inside of the nanorod is quite different from the spheroid. For the spheroid, the field enhancement is uniform across the particle with a value of around 13.4. However, the field enhancement at the center of the nanorod is about 16 and smoothly decreases to about 4

toward its poles [Fig. 9(c)]. Considering that the shape of spheroid is just right to “confine” the electric field to be uniform across the particle, it is not difficult to understand the field distribution in the nanorod on the qualitative basis that the cross section of the nanorod does not shrink toward its poles as fast as the spheroid and therefore the internal electric field is not well confined. In terms of optical nonlinearity due to the internal field enhancement, the nanorod is therefore not as appealing as the spheroid.

### C. Bipyramidal nanoparticles

FDTD calculations are performed on a gold bipyramid defined by Fig. 6(b), with its dimensions  $R=15$  nm,  $h=83.4$  nm, and  $r=3.0$  or  $2.0$  nm. The electric field distribution is calculated at its longitudinal plasmon resonance of 1.534 eV, with the grid resolution set as 0.5 nm [Figs. 10(a) and 10(b)]. In the vicinity of the tips, a large local field enhancement is observed of about a factor of 140. Due to the larger particle size, the field enhancement area extends more broadly into the space compared to the nanorod. In terms of field intensity enhancement, a volume of  $5.5 \times 10^3$  nm<sup>3</sup> presents a field enhancement larger than 1000, and  $5.4 \times 10^4$  nm<sup>3</sup> of space has it larger than 100. The maximum field enhancement is directly related to the curvature of the tip. For a gold bipyramid with sharper tip ( $r=2.0$  nm), the enhancement can be over 200 times at its resonance of 1.503 eV [Fig. 10(c)]. In terms of SERS activity, it would be corresponding to at least  $200^4 = 1.6 \times 10^9$  times of enhancement, where only the electric field contribution is considered.

As we showed earlier, the internal electric field drops quickly toward the poles in the case of nanorod. However, the situation is reversed for the bipyramid. The lowest field enhancement, which is around six times, appears at the center of the bipyramid. For the bipyramid with  $r=2.0$  nm at the poles, the field enhancement grows up to a factor of 30 near the poles [Fig. 10(c)]. The effect is less significant for larger pole radius, but a field enhancement of more than 20 is still observed for bipyramid with  $r=3.0$  nm. It seems that the shape of the bipyramid successfully confines the internal



field so that it rises to very high magnitude toward the poles. We believe such a significant field enhancement offers the opportunity for the study of intrinsic optical nonlinearities in this metal nanoparticle. For instance, in terms of third order nonlinearity, the effect is proportional to the square of the field amplitude. Therefore, the nonlinearity observed in a bipyramid can be four times larger than a spheroid with the same resonance frequency, and much larger than the nanorod.

## V. CONCLUSION

In this paper, we analyzed the optical properties of gold nanorods and bipyramids with the aid of rigorous computational electrodynamics methods. For this purpose, we carried out a variety of FDTD calculations, as well as some DDA calculations. Comparisons with various exact and approximate analytical results, and some experimental results, were also made.

By comparing simulation results on near-field and far-field properties of spheres and spheroids where exact analytical results were available, we deduced criteria for obtaining good accuracy. For achieving the highest accuracy ( $\sim 2\%$ ) at the photon energies ( $\sim 1.5$  eV or 827 nm) of interest, where the magnitude of the metal's dielectric constant is high, the FDTD method was found to be most appropriate. The computationally faster DDA approach, however, is still semi-quantitative ( $\sim 15\%$ ) in this limit and is significantly more accurate at higher energies.

For the FDTD simulations on gold nanorods and pentagonal bipyramids, the computed spectra agreed very well with experimental results. The simulations showed a huge local

electric field enhancement around the poles of the elongated nanostructures at their longitudinal plasmon resonance. The poles with larger curvature showed stronger field enhancement. In particular, the pentagonal bipyramid showed the largest field enhancement of a factor of about 200 making it a promising candidate for enhanced Raman and fluorescence spectroscopies.

Field enhancements within metal nanoparticles have not been discussed much in the literature, but are relevant to understanding metallic nonlinear optical responses. We therefore used the FDTD method to learn about the nature of the electromagnetic fields inside the metal nanoparticles of interest to us. (The DDA approximation was found to give less reliable results concerning these fields.) The field enhancement inside a nanoparticle is found to be very sensitive to its shape. The field amplitude drops quickly toward the poles in the case of nanorod, but increases quickly for the bipyramid, while being nearly uniform for a spheroid. Significant internal field enhancement was found for the gold bipyramid with sharp tips, with the amplitude up to a factor of 30. We thus expect that the field enhancement will lead to pronounced ultrafast optical nonlinearity in this very unique nanostructure.

## ACKNOWLEDGMENTS

This work was supported by the University of Chicago MRSEC NSF-DMR under Grant No. DMR-0213745. S.K.G. was supported by the Office of Basic Energy Sciences, Division of Chemical Sciences, Geosciences, and Biosciences, U.S. Department of Energy under Contract No. DE-AC02-06CH11357.

\*pgs@uchicago.edu

<sup>†</sup>Present address: Center for Computation and Technology, Louisiana State University, Baton Rouge, Louisiana 70803, USA

<sup>‡</sup>gray@tcg.anl.gov

<sup>1</sup>M. Faraday, Philos. Trans. R. Soc. London, Ser. A **147**, 145 (1857).

<sup>2</sup>U. Kreibig and M. Vollmer, *Optical Properties of Metal Clusters* (Springer, Berlin, 1995).

<sup>3</sup>C. F. Bohren and D. R. Huffman, *Absorption and Scattering of Light by Small Particles* (Wiley, New York, 1983).

<sup>4</sup>D. L. Jeanmaire and R. P. Van Duyne, J. Electroanal. Chem. **84**, 1 (1977).

<sup>5</sup>S. Kuhn, U. Håkanson, L. Rogobete, and V. Sandoghdar, Phys. Rev. Lett. **97**, 017402 (2006).

<sup>6</sup>M. Pelton, M. Z. Liu, S. Park, N. F. Scherer, and P. Guyot-Sionnest, Phys. Rev. B **73**, 155419 (2006).

<sup>7</sup>R. C. Jin, Y. W. Cao, C. A. Mirkin, K. L. Kelly, G. C. Schatz, and J. G. Zheng, Science **294**, 1901 (2001).

<sup>8</sup>R. D. Averitt, D. Sarkar, and N. J. Halas, Phys. Rev. Lett. **78**, 4217 (1997).

<sup>9</sup>Y. G. Sun and Y. N. Xia, Science **298**, 2176 (2002).

<sup>10</sup>M. Z. Liu and P. Guyot-Sionnest, J. Phys. Chem. B **109**, 22192 (2005).

<sup>11</sup>N. R. Jana, L. Gearheart, and C. J. Murphy, J. Phys. Chem. B **105**, 4065 (2001).

<sup>12</sup>B. Nikoobakht and M. A. El-Sayed, Chem. Mater. **15**, 1957 (2003).

<sup>13</sup>C. Kittel, *Introduction to Solid State Physics*, 6th ed. (Wiley, New York, 1986).

<sup>14</sup>G. Mie, Ann. Phys. **25**, 377 (1908).

<sup>15</sup>U. Kreibig, Z. Phys. **234**, 307 (1970).

<sup>16</sup>M. I. Mishchenko, J. Opt. Soc. Am. A **8**, 871 (1991).

<sup>17</sup>M. I. Mishchenko, L. D. Travis, and D. W. Mackowski, J. Quant. Spectrosc. Radiat. Transf. **55**, 535 (1996).

<sup>18</sup>E. M. Purcell and C. R. Pennypacker, Astrophys. J. **186**, 705 (1973).

<sup>19</sup>B. T. Draine and P. J. Flatau, J. Opt. Soc. Am. A **11**, 1491 (1994).

<sup>20</sup>K. S. Yee, IEEE Trans. Antennas Propag. **14**, 302 (1966).

<sup>21</sup>A. Taflov and S. C. Hagness, *Computational Electrodynamics: The Finite-Difference Time-Domain Method*, 2nd ed. (Artech House, Boston, 2000).

<sup>22</sup>T. Jensen, L. Kelly, A. Lazarides, and G. C. Schatz, J. Cluster Sci. **10**, 295 (1999).

<sup>23</sup>K. L. Kelly, E. Coronado, L. L. Zhao, and G. C. Schatz, J. Phys. Chem. B **107**, 668 (2003).

<sup>24</sup>E. Hao and G. C. Schatz, J. Chem. Phys. **120**, 357 (2004).

- <sup>25</sup>S. K. Gray and T. Kupka, Phys. Rev. B **68**, 045415 (2003).
- <sup>26</sup>C. Oubre and P. Nordlander, J. Phys. Chem. B **108**, 17740 (2004).
- <sup>27</sup>D. W. Lynch and W. R. Hunter, in *Handbook of Optical Constants of Solids*, edited by E. D. Palik (Academic, Orlando, 1985), pp. 350–357.
- <sup>28</sup>P. B. Johnson and R. W. Christy, Phys. Rev. B **6**, 4370 (1972).
- <sup>29</sup>N. P. Blanchard, C. Smith, D. S. Martin, D. J. Hayton, T. E. Jenkins, and P. Weightman, Phys. Status Solidi C **0**, 2931 (2003).
- <sup>30</sup>B. T. Draine and P. J. Flatau, arXiv:astro-ph/0409262 (unpublished).
- <sup>31</sup>R. Gans, Ann. Phys. **47**, 270 (1915).
- <sup>32</sup>S. Asano and G. Yamamoto, Appl. Opt. **14**, 29 (1975).
- <sup>33</sup>N. V. Voshchinnikov and V. G. Farafonov, Astrophys. Space Sci. **204**, 19 (1993).
- <sup>34</sup>N. Calander and M. J. Willander, J. Appl. Phys. **92**, 4878 (2002).